

Computationally efficient, high-fidelity micromechanics framework using refined 1D models

*Original*

Computationally efficient, high-fidelity micromechanics framework using refined 1D models / Kaleel, Ibrahim; Petrolo, Marco; Waas, A. M.; Carrera, Erasmo. - In: COMPOSITE STRUCTURES. - ISSN 0263-8223. - STAMPA. - 181:(2017), pp. 358-367. [10.1016/j.compstruct.2017.08.040]

*Availability:*

This version is available at: 11583/2680932 since: 2020-04-24T15:46:52Z

*Publisher:*

A. J. M. Ferreira/Elsevier

*Published*

DOI:10.1016/j.compstruct.2017.08.040

*Terms of use:*

This article is made available under terms and conditions as specified in the corresponding bibliographic description in the repository

*Publisher copyright*

Elsevier postprint/Author's Accepted Manuscript

© 2017. This manuscript version is made available under the CC-BY-NC-ND 4.0 license  
<http://creativecommons.org/licenses/by-nc-nd/4.0/>. The final authenticated version is available online at:  
<http://dx.doi.org/10.1016/j.compstruct.2017.08.040>

(Article begins on next page)

# Computationally efficient, high-fidelity micromechanics framework using refined 1D models

I. Kaleel<sup>\*1</sup>, M. Petrolo<sup>†1</sup>, A. M. Waas<sup>‡2</sup>, and E. Carrera<sup>§1</sup>

<sup>1</sup>MUL<sup>2</sup> Group, Department of Mechanical and Aerospace Engineering, Politecnico di Torino,  
Turin, Italy

<sup>2</sup>William E. Boeing Department of Aeronautics and Astronautics, University of Washington,  
Seattle, WA, United States

Submitted to Composite Structures

*Author for correspondence:*

Erasmus Carrera, Professor

MUL<sup>2</sup> Group, Department of Mechanical and Aerospace Engineering,  
Politecnico di Torino,

Corso Duca degli Abruzzi 24,

10129 Torino, Italy,

tel: +39 011 090 6836,

fax: +39 011 090 6899,

e-mail: erasmo.carrera@polito.it

---

<sup>\*</sup>Ph.D. Student, ibrahim.kaleel@polito.it

<sup>†</sup>Assistant Professor, marco.petrolo@polito.it

<sup>‡</sup>Boeing-Egtvedt Chair, Professor of Aerostructures, awaas@aa.washington.edu

<sup>§</sup>Professor of Aerospace Structures and Aeroelasticity, erasmo.carrera@polito.it

## ***Abstract***

*A novel micromechanical framework based on higher-order refined beam models is presented. The micromechanical framework is developed within the scheme of the Carrera Unified Formulation (CUF), a hierarchical formulation which provides a framework to obtain refined structural theories via a variable kinematic description. The Component-Wise approach (CW), a recent extension of one-dimensional (1D) CUF models, is utilized to model components within the representative volume element (RVE). CW models employ Lagrange-type polynomials to interpolate the kinematic field over the element cross-sections of the beams and efficiently handles the analysis of multi-component structures such as RVE. The governing equations are derived in the weak form using finite element method. The framework derives its efficiency from the ability of CUF models to produce accurate displacement and 3D fields at a reduced computational cost. Three different cases of micromechanical homogenization are presented to demonstrate the efficiency and high-fidelity of the proposed framework. The results are validated through published literature results and via the commercial software ABAQUS. The capability of CUF-CW models to accurately predict the overall elastic moduli along with the recovery of local 3D fields is highlighted.*

**Keywords:** Micromechanical homogenization, Carrera Unified Formulation, 1D Models, RVE

# 1 Introduction

With the latest advances in the field of computing power, the viability of virtual testing simulations of advanced heterogeneous material systems has significantly improved over the years. Virtual testing aims at reducing the extensive reliance on empirical testing of such advanced structural systems as well as the associated costs [1]. In addition, the accurate modeling via virtual testing can significantly boost the design space of engineers in the preliminary design phase [2].

The micromechanical analysis is often incorporated into a virtual testing framework to capture sub-scale phenomena such as the fiber-matrix interaction in a fiber reinforced composite system, the honeycomb packing within a sandwich structure, and the non-linear behavior of inclusions in an alloy system. In contrast to macro-scale simulations, the various phases of the material system (geometry and constituent properties) are explicitly modeled through the definition of representative volume elements (RVE). A number of micromechanical theories, including analytical, semi-analytical, and fully-numerical methods, are available in the literature. An extensive review of various kinds of micromechanical homogenization techniques can be found in [3, 4, 5].

Analytical models have been developed to obtain closed-form solutions for effective elastic properties of composites [6, 7, 8, 9] and cellular solids [10] in terms of the constituent properties and the volume fractions. Hashin and Rotem developed bounds and expressions for the effective elastic moduli of reinforced composites by proposing the Concentric Cylinder Model (CCM) [6]. The rules of mixture bounds by Voigt [11] and Reuss [12], Eshelby model [7], Mori-Tanaka scheme [8], and the self-consistent estimate by Hill [9] are extensively applied micromechanical theories for computing the effective elastic moduli of composite materials. Gibson and Ashby [10] proposed a mesomechanics method to evaluate the in-plane effective Young modulus for thin-walled cellular materials. Even though these analytical methods are extensively used for the linear analysis of composite structures, they fail to provide local stress and strain concentrations in the constituent materials. This may hinder the usage of such models for non-linear analysis within the virtual testing framework.

Semi-analytical methods often provide a better prediction of elastic moduli of aforementioned material systems, especially in the case of non-linear analysis. In addition, such methods resolve the local fields at the constituent level, thereby providing better insights into the micromechanical problem in hand. These methods often represent the microstructure of the material by a representative volume element (RVE),

which is partitioned into a number of subregions. Nemat-Nasser et al. expressed the overall moduli of a composite in terms of several infinite series which depend only on the geometry of the void [13]. Fourier series were employed to obtain the local strain fields and bounds on overall elastic and elasto-plastic moduli in [14]. Williams proposed an elasticity-based cell model (ECM) for a periodic array of 3D unit cells [15]. ECM describes the displacement field in each sub-cell via an eigenfunction expansion up to fifth order. Aboudi developed a semi-analytical micromechanics theory based on the analysis of a repeating cell, referred to as the Method of Cells (MOC) [16]. The generalized method of cells (GMC) is an extension of MOC, in which an RVE is subdivided into an arbitrary number of sub-cells with a linearly expanded displacement field [17]. GMC takes into account the fiber packing and the geometry of the RVE. The local stress fields were resolved at the sub-cell level and the effective properties are determined via volume averaging of the local fields. The high-fidelity generalized method of cells (HFGMC) is a recent extension of MOC, in which displacement fields are expanded using second-order approximations [18]. HFGMC can provide accurate local fields within the sub-cell and it has been extensively used for non-linear and failure analysis of composites [19].

Fully numerical methods, such as FEM, are often utilized as micromechanics tool to obtain accurate local fields within the constituent material. Sun and Vaidya provided a rigorous mechanics foundation for predicting the mechanical properties of unidirectional fiber composites [20] using FEM. Heinrich et al. utilized the FEM based RVE analysis to study the influence of fiber packing and the number of fibers on the homogenized response of a cured fiber composite [21]. Yu and Tang proposed the variational asymptotic method for unit cell homogenization (VAMUCH) to predict the effective properties of periodically heterogeneous materials and recover the local fields [22]. The variational statement of the unit cell was formulated through an asymptotic expansion of the energy functional. Even though fully-numerical methods provide accurate descriptions of the local stress, computational limitations often inhibit their application into multi-scale models. Users often come across trade-off between the high-fidelity analysis and the computational requirement. Improved efficiency at the micromechanical level can significantly boost the computational overhead required by such large-scale virtual testing simulation. To circumvent high computational costs, techniques such as order-reduction techniques are employed, in which the order-reduced models approximate the solution to an acceptable error with an increased efficiency [23]. The purpose of the following paper is to present a novel micromechanics framework based on computationally efficient refined beam models. Refined beam models are based on the Carrera Unified Formulation

(CUF) [24], a hierarchical formulation to obtain refined structural theories that account for a variable kinematic description. In particular, the Component-Wise approach (CW) is adopted for modeling micromechanics problem, in which various components of the RVE are modeled via 1D finite elements [25, 26]. CUF models can deal with arbitrary cross-sections, various classes of material models and boundary conditions, without any ad-hoc assumptions, which makes it an ideal candidate for micromechanics analysis. The efficiency of the framework is derived from the ability of CUF models to provide accurate 3D displacement and stress fields at a reduced computational cost (approximately one order of magnitude of degrees of freedom less as compared to standard 3D brick elements) [24, 25, 27]. Over the last couple of decades, CUF models have been extensively used for wide range of structural simulations such as static analysis of laminated beams [28], dynamic response for aerospace structures [29], vibration characteristics of rotating structures [30], evaluation of failure indices in composite structures [26], buckling and post-buckling analysis of compact and composite structures [31, 32]. Carrera et al. reported an extended review of recent developments in refined theories for beam based on CUF with particular focus on diverse applications [33].

The paper is organized as follows: CUF is introduced in Section 2 along with detailed description of the CW. The finite element formulation of the CUF model is described in Section 3. Section 4 describes the proposed Component-Wise micromechanics framework in detail. It also includes aspects pertaining to the numerical implementation of the micromechanics framework. Numerical results are enlisted in Section 5. The concluding remarks are outlined in Section 6.

## 2 Carrera Unified Formulation

The CUF formulates the kinematic field over the cross-section - 1D models such as beams - or along the thickness - 2D models such as plates - in a unified manner. Within the 1D CUF structural models, generic cross-section expansion functions  $F_\tau$  are utilized to define the displacement field, which can be expressed as follows:

$$\mathbf{u}(x, y, z) = F_\tau(x, z)\mathbf{u}_\tau(y), \quad \tau = 1, \dots, M \quad (1)$$

where  $M$  is the number of expansion terms in the cross-section functions  $F_\tau$ , and  $\mathbf{u}_\tau$  is the generalized displacement vector. Unlike the classical models, such as the Euler-Bernoulli Beam Theory (EBBT) and Timoshenko Beam Theory (TBT), the choice of  $F_\tau$  and  $M$  remains arbitrary, and various classes of basis

functions such as polynomial, harmonic or exponential etc. can be adopted as  $F_\tau$ . The theory of structure used in the beam formulation is determined by the type of the expansion function. Over the past few years, three main classes of 1D models have been developed under the umbrella of the CUF, namely: Taylor-based Expansions (TE) [27], Lagrange-based Expansions (LE) [25], and Hierarchical Legendre-based Expansions (HLE) [28].

The micromechanics framework presented in this paper is based on LE, in which  $F_\tau$  is defined using Lagrange polynomials. LE CUF models consist of only displacement unknowns and they were first introduced in [25]. Four types of Lagrange polynomial sets are utilized to define the cross-section expansion, namely: three-point linear (L3), four-point bilinear (L4), nine-point biquadratic (L9), and sixteen-point bicubic (L16) polynomials. In this work, L9 Lagrange polynomials are used to model the cross-section as shown in Fig. 1. The isoparametric formulation is exploited to deal with arbitrary-shaped geometries. The interpolation function for an L9 element can be expressed as

$$\begin{aligned} F_\tau &= \frac{1}{2}(r^2 + rr_\tau)(s^2 + ss_\tau) & \tau = 1, 3, 5, 7 \\ F_\tau &= \frac{1}{2}r_\tau^2(r^2 + rr_\tau)(1 - s^2) + \frac{1}{2}s_\tau^2(s^2 + ss_\tau)(1 - r^2) & \tau = 2, 4, 6, 8 \\ F_\tau &= (1 - r^2)(1 - s^2) & \tau = 9 \end{aligned} \quad (2)$$

where  $r$  and  $s$  vary from  $-1$  to  $+1$  and  $r_\tau$  and  $s_\tau$  are the coordinates of the nine points as illustrated in Fig. 1. The displacement field within an L9 element can be expressed as

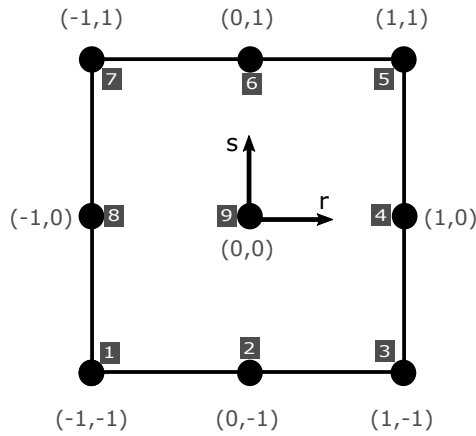


Figure 1: Cross-section L9 element in natural coordinate system

$$\begin{aligned}
u_x &= F_1 u_{x_1} + F_2 u_{x_2} + \dots + F_9 u_{x_9} \\
u_y &= F_1 u_{y_1} + F_2 u_{y_2} + \dots + F_9 u_{y_9} \\
u_z &= F_1 u_{z_1} + F_2 u_{z_2} + \dots + F_9 u_{z_9}
\end{aligned} \tag{3}$$

where  $u_{x_1}, \dots, u_{x_9}$  represent the translational, unknown, displacement components of each of the nine nodes in the L9 element. Multiple L9 elements can be employed for modeling cross-section, thereby allowing local refinements of the kinematic field. The Component-Wise (CW) approach stems out from this very property of the LE-CUF models, in which Lagrange elements are used to model the displacement variables for each component at the cross-sectional level.

### 3 Finite Element Approximation

The strain  $\boldsymbol{\epsilon}$  and stress  $\boldsymbol{\sigma}$  vectors are grouped as follows:

$$\begin{aligned}
\boldsymbol{\epsilon} &= \{\epsilon_{xx} \ \epsilon_{yy} \ \epsilon_{zz} \ \epsilon_{xy} \ \epsilon_{xz} \ \epsilon_{yz}\}^T \\
\boldsymbol{\sigma} &= \{\sigma_{xx} \ \sigma_{yy} \ \sigma_{zz} \ \sigma_{xy} \ \sigma_{xz} \ \sigma_{yz}\}^T
\end{aligned} \tag{4}$$

With small strain assumptions, the linear strain-displacement relations can be given as

$$\boldsymbol{\epsilon} = \mathbf{D} \mathbf{u} \tag{5}$$

where  $\mathbf{D}$  is the linear differential operator on  $\mathbf{u}$  given by

$$\begin{aligned}
\mathbf{D} &= \begin{bmatrix} \frac{\partial}{\partial x} & 0 & 0 \\ 0 & \frac{\partial}{\partial y} & 0 \\ 0 & 0 & \frac{\partial}{\partial z} \\ \frac{\partial}{\partial y} & \frac{\partial}{\partial x} & 0 \\ \frac{\partial}{\partial z} & 0 & \frac{\partial}{\partial x} \\ 0 & \frac{\partial}{\partial z} & \frac{\partial}{\partial y} \end{bmatrix} = \begin{bmatrix} \frac{\partial}{\partial x} & 0 & 0 \\ 0 & 0 & 0 \\ 0 & 0 & \frac{\partial}{\partial z} \\ 0 & \frac{\partial}{\partial x} & 0 \\ \frac{\partial}{\partial z} & 0 & \frac{\partial}{\partial x} \\ 0 & \frac{\partial}{\partial z} & 0 \end{bmatrix} + \begin{bmatrix} 0 & 0 & 0 \\ 0 & \frac{\partial}{\partial y} & 0 \\ 0 & 0 & 0 \\ \frac{\partial}{\partial y} & 0 & 0 \\ 0 & 0 & 0 \\ 0 & 0 & \frac{\partial}{\partial y} \end{bmatrix} \\
&= \mathbf{D}_\Omega + \mathbf{D}_y
\end{aligned} \tag{6}$$



where  $\mathbf{D}_\Omega$  and  $\mathbf{D}_y$  correspond to differential operators for cross-section expansion and beam shape functions. In this work, two types of materials are considered, namely isotropic and orthotropic. Hence, the Hooke law providing the constitutive law holds,

$$\boldsymbol{\sigma} = \mathbf{C} \boldsymbol{\epsilon} \quad (7)$$

where the material matrix  $\mathbf{C}$  is given as

$$\mathbf{C} = \begin{bmatrix} C_{11} & C_{12} & C_{11} & 0 & 0 & 0 \\ C_{21} & C_{22} & C_{23} & 0 & 0 & 0 \\ C_{31} & C_{32} & C_{33} & 0 & 0 & 0 \\ 0 & 0 & 0 & C_{44} & 0 & 0 \\ 0 & 0 & 0 & 0 & C_{55} & 0 \\ 0 & 0 & 0 & 0 & 0 & C_{66} \end{bmatrix} \quad (8)$$

where the coefficients of the material matrix  $\mathbf{C}$  are based on the Young modulus  $E$ , Poisson ratio  $\nu$  and Shear modulus  $G$  of the constituents [34].

The beam is discretized using the finite element approach along  $y$ , as shown in Fig. 2. Via the classical finite element technique, the displacement vector (Eq. 1) can be reformulated as

$$\mathbf{u}(x, y, z) = F_\tau(x, z) N_i(y) \mathbf{u}_{\tau i}, \quad \tau = 1, \dots, M, \quad i = 1, \dots, p + 1 \quad (9)$$

where  $N_i$  stands for the shape function of order  $p$  and  $\mathbf{u}_{\tau i}$  is the nodal displacement vector. In this work, beam elements with four nodes (B4), i.e. a cubic approximation, are adopted. For the sake of brevity, the shape functions are not reported, the reader is referred to the book by Bathe [35]. The discretization of the cross-section of the beam element remains independent of the choice of the beam finite element used. By adopting the Principle of Virtual Displacement (PVD), the governing equations for a static response hold the following

$$\delta L_{int} = \delta L_{ext} \quad (10)$$

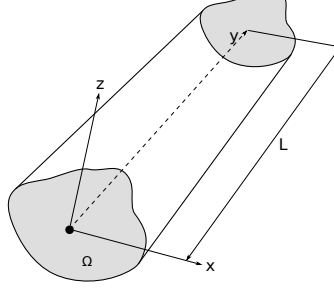


Figure 2: Coordinate frame of reference for a generic beam

where  $\delta L_{int}$  and  $\delta L_{ext}$  are the virtual variation of internal work and work due to external loading respectively. The internal work can be expressed as

$$\delta L_{int} = \int_l \int_{\Omega} \delta \boldsymbol{\epsilon}^T \boldsymbol{\sigma} d\Omega dy \quad (11)$$

where  $l$  and  $\Omega$  are the length of the beam and area of the cross-section, respectively. The virtual variation of internal work (Eq. 11) can be rewritten using the geometrical relation (Eq. 6) and the constitutive law (Eq. 8) as follows:

$$\begin{aligned} \delta L_{int} &= \delta \mathbf{u}_{js}^T \int_l \int_{\Omega} [N_j(y) F_s(x, z) \mathbf{D}^T \mathbf{C} \mathbf{D} F_{\tau}(x, z) N_i(y)] d\Omega dl \\ &= \delta \mathbf{u}_{js}^T \mathbf{K}_{ij\tau s} \mathbf{u}_{i\tau} \end{aligned} \quad (12)$$

where  $\mathbf{K}_{ij\tau s}$  is the fundamental nucleus of the stiffness matrix of size  $3 \times 3$ . Indices  $i$  and  $j$  correspond to the beam shape functions  $N_i$  and  $N_j$ , respectively;  $\tau$  and  $s$  are related to the cross-section expansion functions  $F_{\tau}$  and  $F_s$ , respectively. The explicit expressions of the nine components of the fundamental nucleus are not repeated here but are given in the book by Carrera et al. [24], with detailed information on the implementation aspects.

## 4 Component-Wise Micromechanics framework

An illustration of the CW modeling of a three-phase triply periodic microstructure is depicted in Fig. 3. The RVE is modeled as a beam structure with the cross-section discretized into an arbitrary number of Lagrange elements along the  $x_2$ - $x_3$  plane. Multiple Lagrange elements with different constitutive properties can be assembled to construct the cross-section of the RVE. This enables the displacement

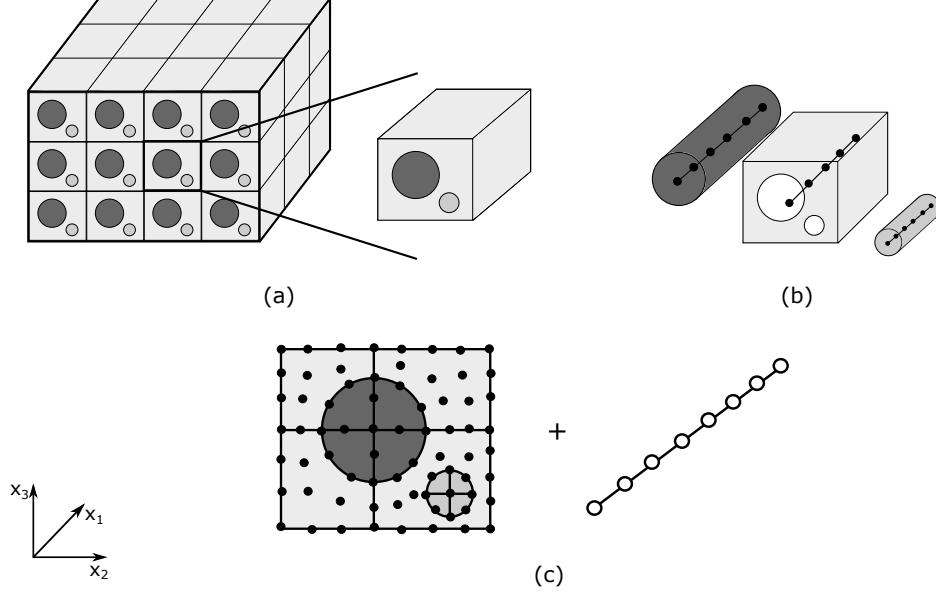


Figure 3: An illustration of a component-wise modeling of composite microstructure with arbitrary constituents (a) a triply periodic composite microstructure with three different phases, (b) Component-Wise modeling of a triply periodic RVE with individual components modeled as separate components and (c) assembled cross-section with Lagrange elements along with the beam for the RVE

continuity across the interface of different constituents. The cross-section extends along the span of the beam in  $x_1$  direction. The beam is modeled using B4 elements (cubic interpolation). The framework is also capable of including span-wise heterogeneity.

The micromechanical framework is formulated based on the periodic nature of the RVE. To ensure the compatibility of displacements along the faces of the RVE, periodic boundary conditions (PBCs) need to be applied [36, 20]. The displacements applied on the faces of the RVE must maintain the energy equivalence between the actual heterogenous material and the homogenized medium [20]. The displacements along the opposite boundary surfaces of the RVE can be formulated as

$$u_i^{j+}(x, y, z) - u_i^{j-}(x, y, z) = \bar{\epsilon}_{ik}(x_k^{j+} - x_k^{j-}) \quad (13)$$

where  $\bar{\epsilon}_{ik}$  is the average strains, indices  $j+$  and  $j-$  represent the positive and negative directions along  $X_k$ . Based on the rigorous mechanical foundation laid by Sun and Vaidya [20], the average strains ( $\bar{\epsilon}_{ij}$ )

and stresses ( $\bar{\sigma}_{ij}$ ) the RVE are given by:

$$\begin{aligned}\bar{\epsilon}_{ij} &= \frac{1}{V} \int_V \epsilon_{ij} dV \\ \bar{\sigma}_{ij} &= \frac{1}{V} \int_V \sigma_{ij} dV\end{aligned}\tag{14}$$

where  $\epsilon_{ij}$  and  $\sigma_{ij}$  are the local strains and local stresses within the individual constituents of the RVE, respectively. The overall material matrix of the homogenized RVE can be formulated as

$$\bar{\sigma}_{ij} = \bar{\mathbf{C}}_{ijkl} \bar{\epsilon}_{ij}\tag{15}$$

where  $\bar{\mathbf{C}}_{ijkl}$  is the homogenized material matrix of the RVE.

As illustrated in Fig. 4, the application of PBCs can be classified into two categories: (1) PBC over the cross-section degrees of freedom and (2) PBC over the end nodes of the beam. Taking the applied strain

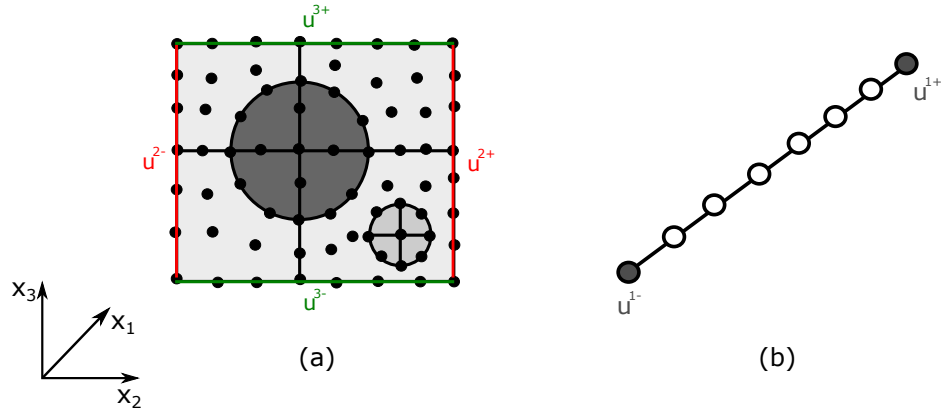


Figure 4: Periodic boundary conditions applied for the (a) cross-section of the beam and (b) end nodes of the beam

as  $\epsilon_{ij}^m$ , the explicit expressions for the PBCs for the cross-section degrees of freedom is expressed as

$$\begin{aligned}
u_{2+}^1 - u_{2-}^1 &= \epsilon_{22}^m l_2 \\
u_{2+}^2 - u_{2-}^2 &= 2 \epsilon_{21}^m l_2 \\
u_{2+}^3 - u_{2-}^3 &= 2 \epsilon_{23}^m l_2 \\
u_{3+}^1 - u_{3-}^1 &= \epsilon_{33}^m l_3 \\
u_{3+}^2 - u_{3-}^2 &= 2 \epsilon_{31}^m l_3 \\
u_{3+}^3 - u_{3-}^3 &= 2 \epsilon_{32}^m l_3
\end{aligned} \tag{16}$$

where  $u_{x+}^k$  represents the degrees of freedom associated with dimension  $x$  along the positive direction of  $k$ ,  $l_2$  and  $l_3$  are the lengths of the cross-section along  $x_2$  and  $x_3$ , respectively. These boundary conditions are applied at the cross-section associated with each beam node. PBCs for the beam end nodes are expressed as

$$\begin{aligned}
u_{1+}^1 - u_{1-}^1 &= \epsilon_{11}^m L \\
u_{1+}^2 - u_{1-}^2 &= 2 \epsilon_{12}^m L \\
u_{1+}^3 - u_{1-}^3 &= 2 \epsilon_{13}^m L
\end{aligned} \tag{17}$$

where  $u_{1+}^k$  and  $u_{1-}^k$  are the degrees of freedom associated with positive and negative end nodes of the beam element along the direction  $k$ , and  $L$  is the length of the beam element. The overall system of equation is of the form:

$$\mathbf{K}\mathbf{u} = \mathbf{f} \tag{18}$$

where  $\mathbf{K}$  is the symmetric-sparse matrix obtained via assembly of CUF fundamental nuclei and matrix  $\mathbf{f}$  is of the size  $N \times 6$ , where each one of the 6 columns contain the contributions of the individual applied strain  $\epsilon^m$ , in which  $N$  is the number of degrees of freedom of the model.

## 5 Numerical Results

CUF-CW is utilized to undertake homogenization and de-homogenization analyses of fiber-reinforced composites, void-filled composites, and periodic cellular structures. The predicted values are compared

against reference solutions from literature and 3D finite element models.

## 5.1 Fiber reinforced composites

### A. Effective moduli

The effective moduli of uni-directional fiber reinforced composites are examined in this section. Two cases of fiber reinforced composites, which are extensively studied in the literature, are considered, namely Boron/Aluminum and Graphite/Epoxy material systems. A square packed RVE is modeled. Table 1 enlists the material properties of the constituents for the two uni-directional composites. The fiber volume fractions for Boron/Aluminium and Graphite/Epoxy were 47% and 60%, respectively. Figure 5 shows the

Table 1: Material properties of fiber reinforced composite constituents

| Material        | $E_{11}$<br>(GPa) | $E_{22}$<br>(GPa) | $G_{12}$<br>(GPa) | $\nu_{12}$<br>(-) | $\nu_{23}$<br>(-) |
|-----------------|-------------------|-------------------|-------------------|-------------------|-------------------|
| Boron fiber     | 379.3             | 379.3             | 172.41            | 0.1               | 0.1               |
| Graphite fiber  | 235.0             | 14.0              | 28.0              | 0.2               | 0.25              |
| Aluminum matrix | 68.3              | 68.3              | 26.3              | 0.3               | 0.3               |
| Epoxy matrix    | 4.8               | 4.8               | 1.8               | 0.34              | 0.34              |

CW discretization of the cross-section of the RVE for the Boron/Aluminium and Graphite/Epoxy material systems. The cross-section of the RVE contains 20 L9 elements. The beam is discretized using two B4 elements, essentially summing to a global system with 1869 DOFs. Table 2 and 3 compare the effective properties predicted by the CUF-CW against the results available from literature. Comparisons are made between the finite element approach by Sun and Vaidya [20], Concentric Cylinder model (CCM) developed by Rotem and Hashin [6], Method of Cells (MOC) by Aboudi [16], Generalized Method of Cells (GMC) by Paley and Aboudi [17], High Fidelity Generalized Method of Cells (HFGMC) by Aboudi [18], Elasticity based Cell Method (ECM) by Williams [15], and Variational Asymptotic Method for Unit Cell Homogenization (VAMUCH) by Yu and Tang [22].

### B. Effect of fiber packing

To expand further on the capabilities of the CUF-CW, a study on the effect of fiber packing on the effective moduli of the RVE is undertaken. As depicted in Fig. 6, two classes of RVE architectures are considered for the study, namely square packed and hex-packed RVEs. The square packed and hex-packed RVEs are

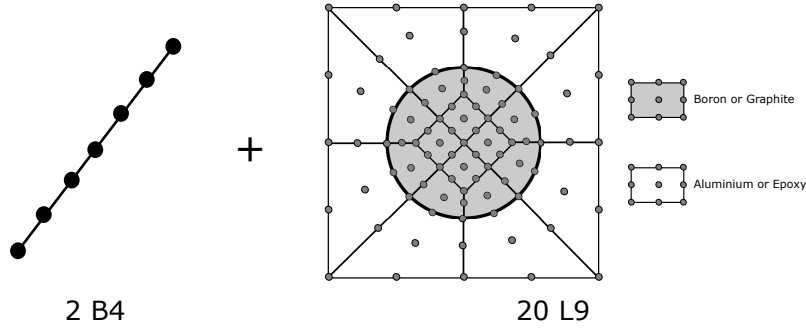


Figure 5: CW discretization of the square packed RVE for analysis of Boron/Aluminium and Graphite/Epoxy material systems

Table 2: Predicted effective material properties of Boron/Aluminum composites

| Models                | $E_{11}$<br>(GPa) | $E_{22}$<br>(GPa) | $G_{12}$<br>(GPa) | $G_{23}$<br>(GPa) | $\nu_{12}$<br>(-) | $\nu_{23}$<br>(-) |
|-----------------------|-------------------|-------------------|-------------------|-------------------|-------------------|-------------------|
| CUF-CW                | 215.2             | 144.3             | 54.4              | 46.0              | 0.195             | 0.253             |
| FEM [20]              | 215.0             | 144.0             | 57.2              | 45.9              | 0.190             | 0.290             |
| CCM [6]               | 231.9             | 127.3             | 54.0              | 49.6              | 0.193             | 0.282             |
| MOC [16]              | 215.0             | 142.6             | 51.3              | 43.7              | 0.200             | 0.250             |
| GMC [17]              | 215.0             | 141.0             | 51.2              | 43.7              | 0.197             | 0.261             |
| HFGMC [18]            | 215.4             | 144.0             | 54.3              | 45.8              | 0.195             | 0.255             |
| ECM ( $3^{rd}$ ) [15] | 215.0             | 143.4             | 54.3              | 45.1              | 0.190             | 0.260             |
| VAMUCH [22]           | 215.0             | 144.1             | 54.4              | 45.9              | 0.195             | 0.255             |

Table 3: Predicted effective material properties of Graphite/Epoxy composites

| Models                | $E_{11}$<br>(GPa) | $E_{22}$<br>(GPa) | $G_{12}$<br>(GPa) | $G_{23}$<br>(GPa) | $\nu_{12}$<br>(-) | $\nu_{23}$<br>(-) |
|-----------------------|-------------------|-------------------|-------------------|-------------------|-------------------|-------------------|
| CUF-CW                | 142.8             | 9.6               | 6.10              | 3.13              | 0.252             | 0.349             |
| FEM [20]              | 142.6             | 9.6               | 6.00              | 3.10              | 0.250             | 0.350             |
| CCM [6]               | 144.6             | 8.9               | 5.8               | 3.3               | 0.252             | 0.361             |
| MOC [16]              | 143.0             | 9.6               | 5.47              | 3.08              | 0.250             | 0.350             |
| GMC [17]              | 143.0             | 9.5               | 5.68              | 3.03              | 0.253             | 0.358             |
| HFGMC [18]            | 142.9             | 9.6               | 6.09              | 3.10              | 0.252             | 0.350             |
| ECM ( $3^{rd}$ ) [15] | 143.0             | 9.6               | 5.85              | 3.07              | 0.250             | 0.350             |
| VAMUCH [22]           | 142.9             | 9.6               | 6.10              | 3.12              | 0.252             | 0.350             |

modeled using 20 L9 and 44 L9 elements, respectively. The beam is discretized using 2 B4 elements.

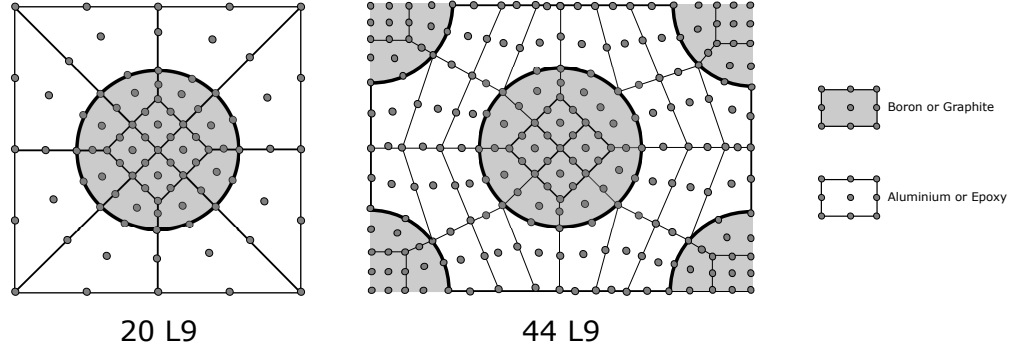


Figure 6: CW discretization of the square packed and hex-packed RVE for analysis of Boron/Aluminium and Graphite/Epoxy material systems

Table 4: Comparison of elastic moduli for different RVE architecture for Boron/Aluminium and Graphite/Epoxy material system

|            | <b>Boron/Aluminium</b> (Fiber VF=47%) |          |            |          | <b>Graphite/Epoxy</b> (Fiber VF=60%) |          |            |          |
|------------|---------------------------------------|----------|------------|----------|--------------------------------------|----------|------------|----------|
|            | Square-packed                         |          | Hex-packed |          | Square-packed                        |          | Hex-packed |          |
|            | CUF-CW                                | FEM [20] | CUF-CW     | FEM [20] | CUF-CW                               | FEM [20] | CUF-CW     | FEM [20] |
| $E_1$      | 215.22                                | 215.0    | 215.19     | 215.0    | 142.83                               | 142.60   | 142.83     | 142.6    |
| $E_2$      | 144.29                                | 144.0    | 132.91     | 136.5    | 9.63                                 | 9.60     | 9.17       | 9.20     |
| $\nu_{12}$ | 0.19                                  | 0.19     | 0.19       | 0.19     | 0.25                                 | 0.25     | 0.25       | 0.25     |
| $\nu_{23}$ | 0.25                                  | 0.29     | 0.31       | 0.34     | 0.35                                 | 0.35     | 0.38       | 0.38     |
| $G_{12}$   | 54.44                                 | 57.2     | 54.18      | 54.0     | 6.10                                 | 6.00     | 5.86       | 5.88     |
| $G_{23}$   | 46.03                                 | 45.9     | 51.13      | 52.5     | 3.13                                 | 3.10     | 3.34       | 3.35     |

### C. De-homogenization of randomly distributed fiber composite

The capability of the CUF-CW micromechanics module to produce accurate stress fields with a reduced computational overhead is illustrated. An RVE of a fiber/matrix composite with 13 randomly distributed fibers (fiber volume fraction of 60%) is modeled using CW approach. The RVE architecture ( $21.25\mu m \times 21.25\mu m$ ) is obtained from the work of Pineda et. al., where progressive damage analysis of the fiber/matrix composite RVE is reported [19]. The fiber is assumed to be made of transversely isotropic graphite fiber, and matrix as linearly isotropic epoxy with properties listed in Table 1. The



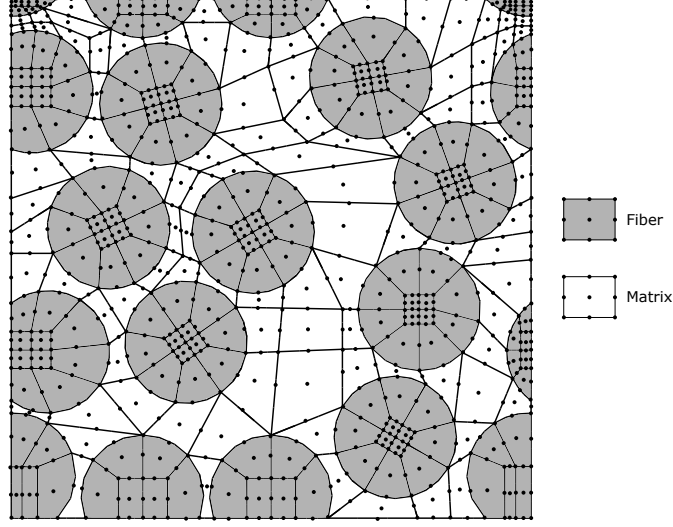


Figure 7: CW discretization of the cross-section of RVE with 13 randomly distributed fibers and a fiber volume fraction of 60%

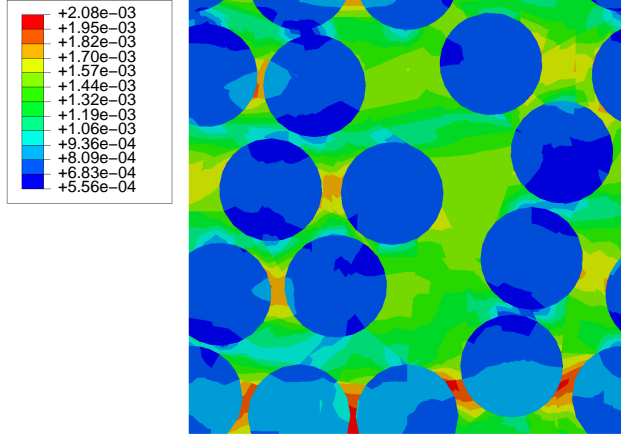
cross-section is modeled using 265 L9 elements as depicted in Fig. 7, and 2 B4 elements were used. The total degrees of freedom of the problem amounts to a sparse system of 19080. A similar RVE model is developed in ABAQUS using 3D brick element using 24765 brick elements with total degrees of freedom of 91305. A global transverse tensile strain ( $\epsilon_{22}$ ) of 0.001 is applied to the RVE. The numerical results for the de-homogenization analysis are enlisted in Table 5. Figures 8-9 depicts the maximum principal strain ( $\epsilon_1$ ) and stress contours ( $\sigma_{22}$ ) for the RVE obtained from CUF-CW and ABAQUS-3D analysis.

Table 5: Numerical results from de-homogenization of RVE with 13 randomly distributed fibers subjected to transverse tensile strain

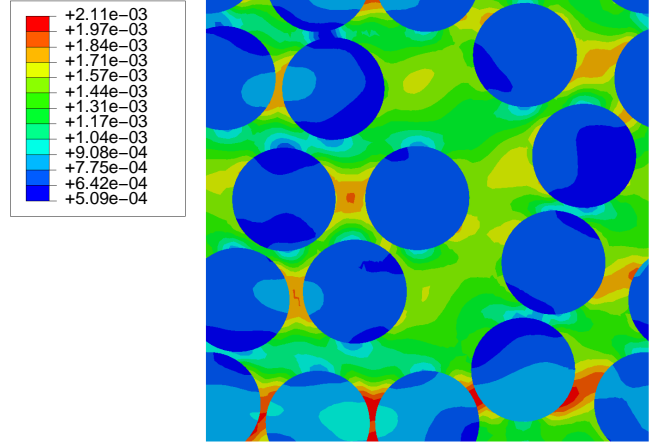
|           | DOF<br>(-) | Maximum principal strain ( $\epsilon_1^{max}$ )<br>$10^{-3}$ | Maximum transverse stress ( $\sigma_{22}^{max}$ )<br>(MPa) |
|-----------|------------|--|--|
| CUF-CW    | 19080      | 2.08   | 14.92  |
| ABAQUS 3D | 91305      | 2.11   | 14.22  |

Results suggests that

- CUF-CW models are able to predict the effective properties of the aforementioned material system accurately.
- The model is able to capture the effect of packing in composite materials.
- Effective transverse moduli of the composite are more vulnerable to the packing architecture of the

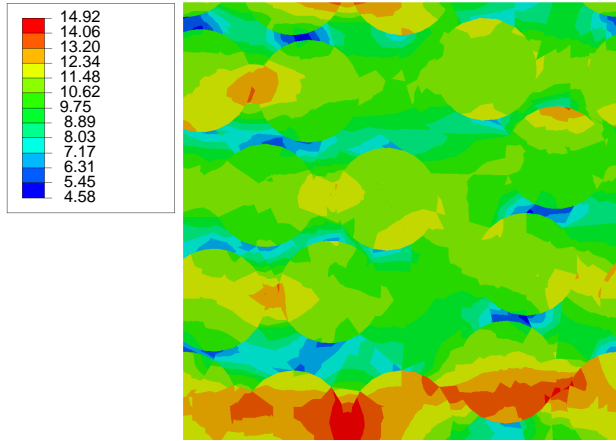


(a) CUF-CW (19080 DOFs)

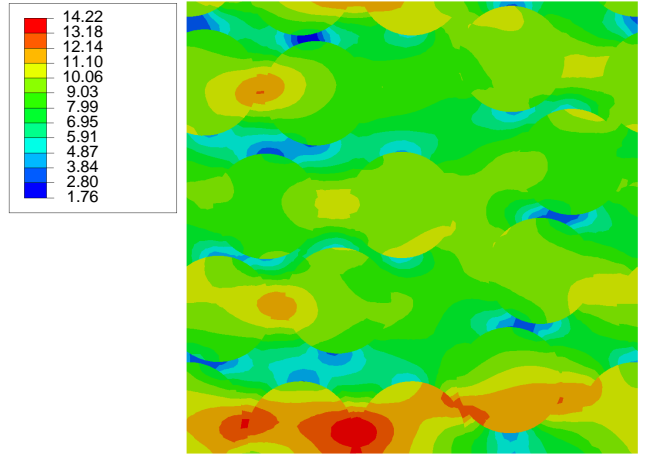


(b) ABAQUS 3D - (91305 DOFs)

Figure 8: Maximum principal strain contours  $\epsilon_1^p$  over the cross-section of the RVE with 13 randomly distributed fibers subjected to transverse tensile strain (a) CW-CUF model and (b) ABAQUS 3D model



(a) CUF-CW (19080 DOFs)



(b) ABAQUS 3D - (91305 DOFs)

Figure 9: Transverse stress contours  $\sigma_{22}$  [MPa] over the cross-section of the RVE with 13 randomly distributed fibers subjected to transverse tensile strain (a) CW-CUF model and (b) ABAQUS 3D model

RVE.

- The de-homogenization analysis of randomly distributed fiber RVEs demonstrates the high-fidelity and efficiency of the framework.

## 5.2 Void filled composite

In the following example, CUF-CW is employed to simulate the global and local behavior of void-filled composites. As depicted in Fig. 10, two kinds of inclusion shapes are investigated, namely square and circular. The beam is discretized using 2 B4 element and the degrees of freedom of the global linear system accounts to 4032 and 3780 for circular and square voided composites, respectively. The void filled composite is made of copper with Young modulus  $E = 127.0 \text{ GPa}$  and Poisson ratio  $\nu = 0.34$ . Table 6 enlists the effective transverse Young modulus predicted for different void volume fractions of

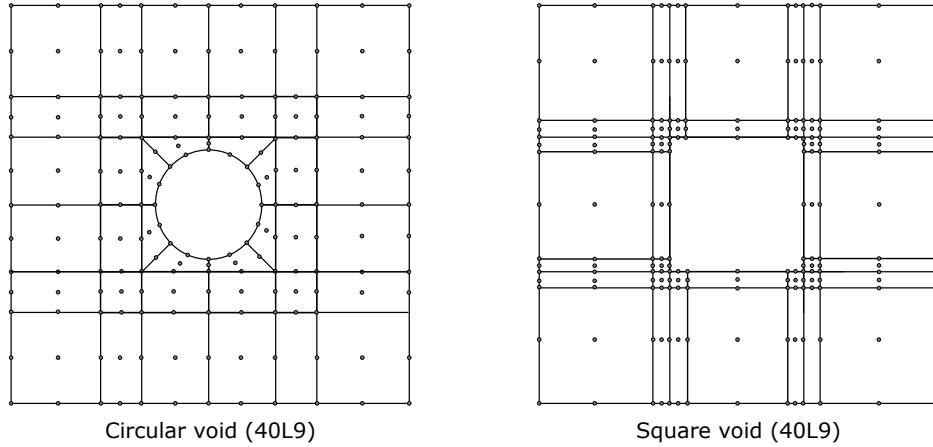


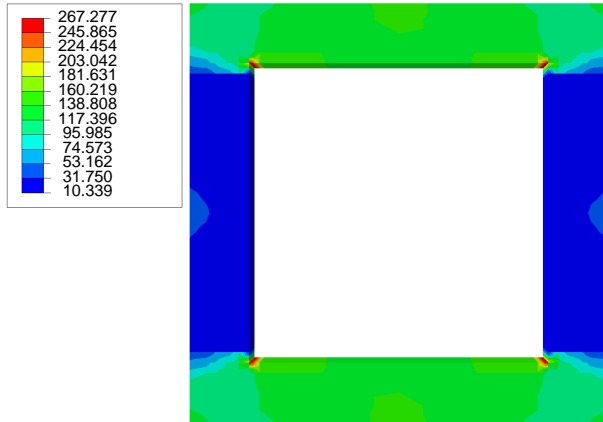
Figure 10: CW discretization of the circular and square void for analysis of void filled Cu composite

0.0204, 0.1837, 0.5102 and 0.7511. The predicted values are compared against Method of Cells (MOC) by Aboudi [16], Elasticity-based Cell Method (ECM) ( $3^{rd}$  and  $5^{th}$  order) by Williams [15], and Variational Asymptotic Method for Unit Cell Homogenization (VAMUCH) by Yu and Tang [22].

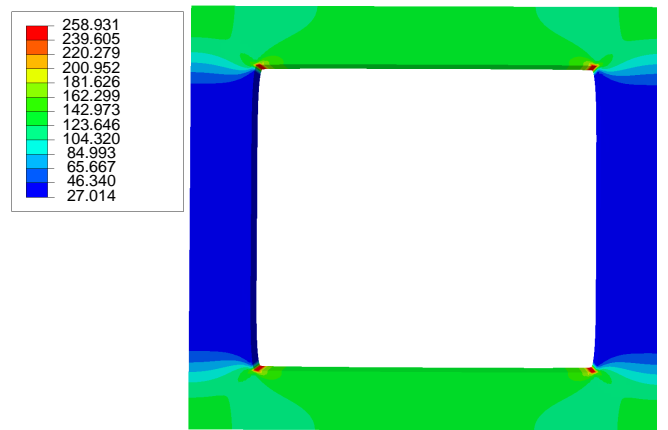
Square inclusions exhibit strong gradients due to stress concentration around the corner. To highlight the computational efficiency obtained via CUF-CW, a FEM model using 3D brick element (C3D8) was developed in ABAQUS for the square inclusion with a void volume fraction of 0.5102. The RVE is subjected to a transverse tensile strain ( $\epsilon_{11}$ ) of 0.001. The von-Mises stress contour over the cross-section of the RVE is depicted in Fig. 11. The ABAQUS 3D model has 72225 DOFs, the CUF-CW 3456. The results suggest that

Table 6: Predicted transverse Young modulus  $E_{22}$  (GPa) of void-filled Cu composite with varying void volume fraction

|                      | Void volume fraction |        |        |        |
|----------------------|----------------------|--------|--------|--------|
|                      | 0.0204               | 0.1837 | 0.5102 | 0.7511 |
| <b>Circular void</b> |                      |        |        |        |
| CUF-CW               | 120.36               | 82.27  | 39.57  | 10.32  |
| VAMUCH [22]          | 120.34               | 82.67  | 39.08  | 10.31  |
| FEM [22]             | 120.34               | 82.64  | 39.08  | 10.31  |
| <b>Square void</b>   |                      |        |        |        |
| CUF-CW               | 120.22               | 82.02  | 39.85  | 18.28  |
| MOC [16]             | 110.20               | 75.27  | 38.22  | 17.99  |
| G-F [37]             | 120.63               | 83.50  | 40.48  | 18.40  |
| ECM (3rd)[15]        | 110.20               | 75.38  | 38.23  | 17.99  |
| ECM (5th)[15]        | 118.90               | 80.97  | 39.64  | 18.20  |
| VAMUCH [22]          | 120.22               | 81.73  | 39.75  | 18.25  |
| FEM [22]             | 120.22               | 81.70  | 39.75  | 18.25  |



(a) CW-CUF model (3456 DOFs)



(b) ABAQUS 3D - (72225 DOFs)

Figure 11: von-Mises stress contours  $\sigma_{vm}$  [MPa] over the cross-section of the RVE of void-filled Cu composite with a void volume fraction of 0.5102 subjected to transverse tensile strain ( $\epsilon_{11}$ ): (a) CUF-CW and (b) ABAQUS 3D

- CUF-CW models can predict the transverse Young modulus accurately.
- CUF-CW models can capture the strong stress gradients observed along the edges of the square-inclusion.

### 5.3 Periodical cellular material

The section focuses on the prediction of the effective Young modulus for periodical cellular materials using CUF-CW. As depicted in Fig. 12(a), the architecture of the RVE is of hexagonal honeycomb. The dimensions of the hexagonal honeycomb RVE is tabulated in Table 7. The material of the RVE is assumed to be isotropic with the Young modulus  $E_0$  of 0.91 GPa and Poisson ratio  $\nu$  of 0.3. The RVE is

Table 7: Dimensions of hexagonal honeycomb RVE

| $a$        | $t/a$                 | $\phi$     |
|------------|-----------------------|------------|
| $3^{-3/4}$ | $\frac{\sqrt{3}}{12}$ | $60^\circ$ |

modeled using 28L9 elements as shown Fig. 12(b). In order to stay consistent with the micromechanical formulation, the void areas (white areas in 12(b)) are modeled with a weak material with very low stiffness ( $E_{void}/E_0 = 10^{-5}$ ). The RVE is discretized using 2B4 elements along the longitudinal axis and the total degrees of freedom of the system amounts to 6993 (includes the additional degrees of freedom due to void elements). Table 8 enlists the predicted transverse Young modulus and compares against the reference and ABAQUS 3D solutions.

A de-homogenization analysis is undertaken with RVE being subject to transverse strain ( $\epsilon_{33}$ ) of 0.001. Maximum principal strain ( $\epsilon_1^p$ ) contour and von-Mises stress ( $\sigma_{vm}$ ) are depicted in Fig. 13 and Fig. 14, respectively. An ABAQUS 3D model with 79104 DOFs was used, whereas CUF-CW 6993.

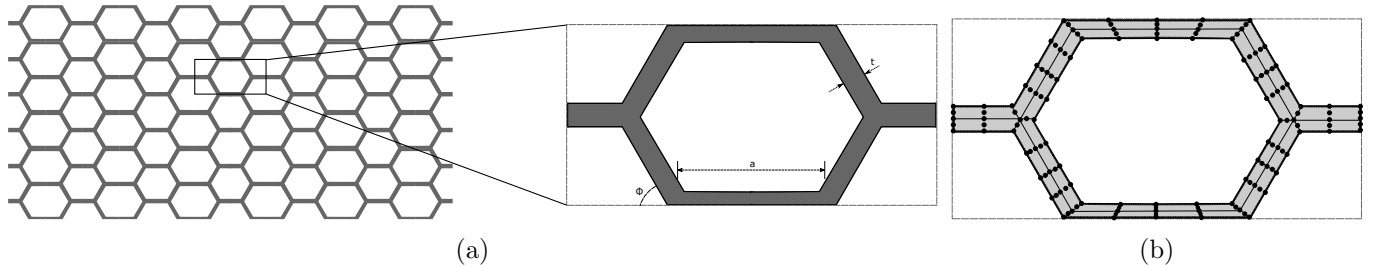


Figure 12: Architecture of hexagonal honeycomb RVE: (a) Dimensions of the hexagonal honeycomb RVE and (b) CW discretization of the cross-section for hexagonal honeycomb RVE using 18L9 elements

Table 8: Predicted tranverse Young modulus  $E_{22}$  (GPa) of the cellular hexagonal honeycomb RVE

| CUF-CW | G-A MMM | FEM 3D |
|--------|---------|--------|
| 0.0504 | 0.0498  | 0.0485 |

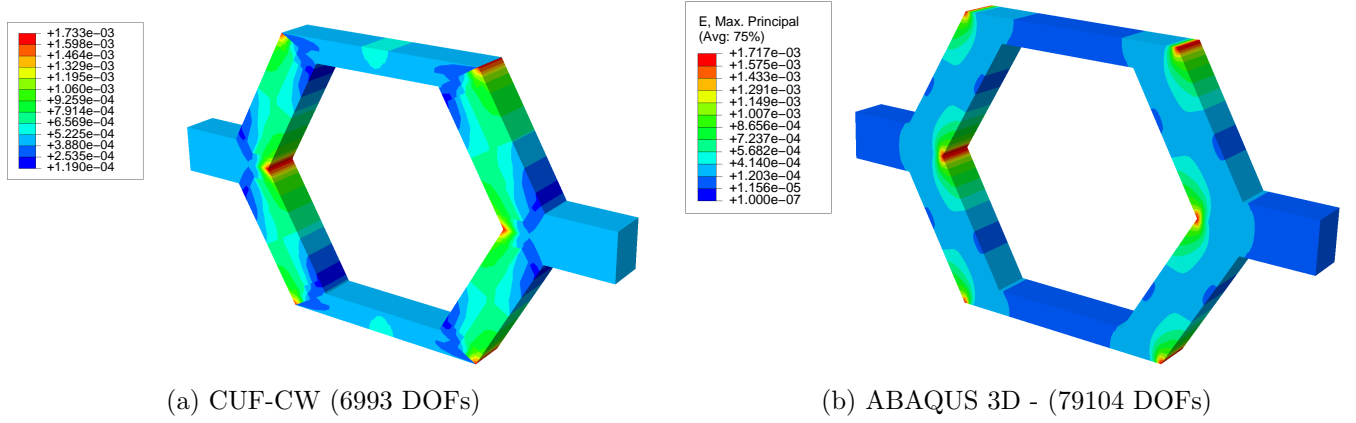


Figure 13: Maximum principal strain contours  $\epsilon_1^p$  for hexagonal honeycomb RVE with subjected to transverse tensile strain ( $\epsilon_{33}$ ) (a) CW-CUF model and (b) ABAQUS 3D model

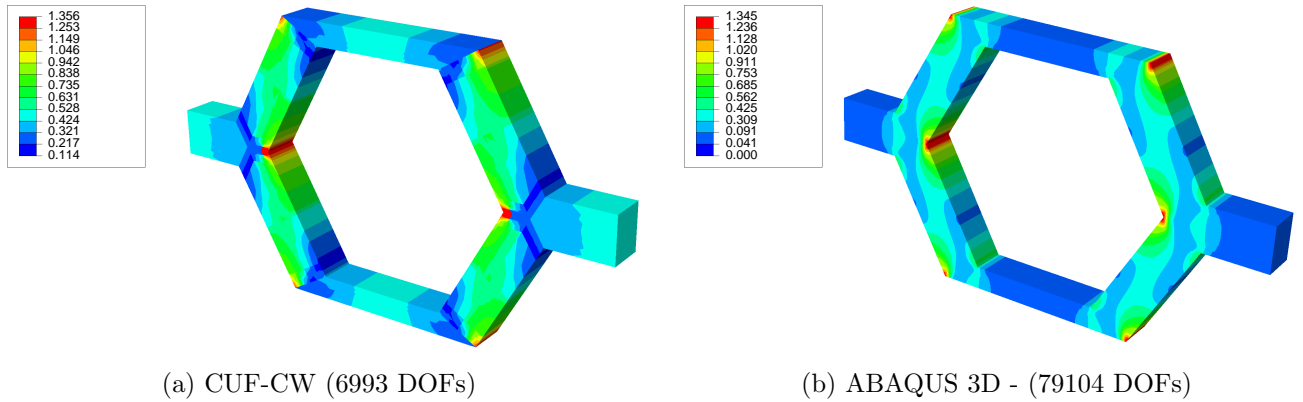


Figure 14: von-Mises stress contours  $\sigma_{vm}$  [MPa] for hexagonal honeycomb RVE with subjected to transverse tensile strain ( $\epsilon_{33}$ ) (a) CW-CUF model and (b) ABAQUS 3D model

Results suggests that

- In comparison to the reference solution and FEM 3D results, CUF-CW can predict the transverse Young modulus accurately.
- CUF-CW can effectively capture strong gradients within the honeycomb RVE.

## 6 Conclusion

A novel and computationally efficient micromechanics framework based on refined beam models is presented. The framework is built within the scheme of the Carrera Unified Formulation (CUF), a generalized hierarchical formulation which yields a refined structural theory via variable kinematic description. The representative volume element (RVE) is modeled using the Component-Wise approach (CW), an extension of the CUF beam model based on Lagrange type polynomials. The versatility of the framework is demonstrated through numerical results taken from the literature for fiber-reinforced composites, void-filled composites, and periodic cellular material. The efficiency of the framework is highlighted by comparing the total number of degrees of freedom of the global system of CUF-CW models against ABAQUS 3D results. Following conclusions can be drawn:

1. CUF-CW can accurately predict the effective elastic moduli of the three cases presented.
2. CUF-CW is able to recover the 3D fields accurately and efficiently.
3. On average, CUF-CW requires one order of magnitude of degrees of freedom less compared to standard 3D brick elements to obtain similar results.
4. The high fidelity of the framework is demonstrated through de-homogenization analysis of randomly distributed fiber-reinforced composites.

It can be concluded that CUF-CW provides a reliable and efficient tool to accurately undertake micromechanics analysis. Future works will deal with the extension of the tool for the non-linear analysis, such as progressive damage analysis.

## 7 Acknowledgement

This research work has been carried out within the project FULLCOMP (FULLy analysis, design, manufacturing, and health monitoring of COMposite structures), funded by the European Union Horizon 2020 Research and Innovation program under the Marie Skłodowska-Curie grant agreement No. 642121.

## References

- [1] J. Llorca, C. González, J. M. Molina-Aldareguía, J. Segurado, R. Seltzer, F. Sket, M. Rodríguez, S. Sádaba, R. Muñoz, and L. P. Canal. Multiscale modeling of composite materials: A roadmap towards virtual testing. *Advanced Materials*, 23(44):5130–5147, 2011.
- [2] B. Cox and Q. Yang. In quest of virtual tests for structural composites. *Science (New York, N.Y.)*, 314(November):1102–1107, 2006.
- [3] S. J. Hollister and N. Kikuchi. A comparison of homogenization and standard mechanics analyses for periodic porous composites. *Computational Mechanics*, 10(2):73–95, 1992.
- [4] C. T. Herakovich. Mechanics of composites: A historical review. *Mechanics Research Communications*, 41:1–20, 2012.
- [5] B. Hassani and E. Hinton. A review of homogenization and topology optimization II analytical and numerical solution of homogenization equations. *Computers & Structures*, 69(6):719–738, 1998.
- [6] ZVI. Hashin and B. W. Rosen. The Elastic Moduli of Fiber-Reinforced Materials. *Journal of Applied Mechanics*, 31(2):223–232, 1964.
- [7] J. D. Eshelby. The determination of the elastic field of an ellipsoidal inclusion, and related problems. *Proceedings of the Royal Society of London A: Mathematical, Physical and Engineering Sciences*, 241(1226):376–396, 1957.
- [8] T. Mori and K. Tanaka. Average stress in matrix and average elastic energy of materials with misfitting inclusions. *Acta Metallurgica*, 21(5):571 – 574, 1973.
- [9] R. Hill. A self-consistent mechanics of composite materials. *Journal of the Mechanics and Physics of Solids*, 13(4):213 – 222, 1965.



- [10] L. J. Gibson and M. F. Ashby. *Cellular Solids: Structure and Properties*. Cambridge University Press, 1999.
- [11] W. Voigt. Ueber die beziehung zwischen den beiden elasticitätsconstanten isotroper körper. *Annalen der Physik*, 274(12):573–587, 1889.
- [12] A. Reuss. Berechnung der fliegrenze von mischkristallen auf grund der plastizitätsbedingung fr einkristalle . *ZAMM Journal of Applied Mathematics and Mechanics / Zeitschrift fr Angewandte Mathematik und Mechanik*, 9(1):49–58, 1929.
- [13] S. Nemat-Nasser, T. Iwakuma, and M. Hejazi. On composites with periodic structure. *Mechanics of Materials*, 1(3):239 – 267, 1982.
- [14] M. L. Accorsi and S. Nemat-Nasser. Bounds on the overall elastic and instantaneous elastoplastic moduli of periodic composites. *Mechanics of Materials*, 5(3):209 – 220, 1986.
- [15] T. O. Williams. A three-dimensional, higher-order, elasticity-based micromechanics model. *International Journal of Solids and Structures*, 42(3-4):971–1007, 2005.
- [16] J. Aboudi. A continuum theory for fiber-reinforced elastic-viscoplastic composites. *International Journal of Engineering Science*, 20(5):605–621, 1982.
- [17] M. Paley and J. Aboudi. Micromechanical Analysis of Composites by the Method of Cells. *Applied Mechanics Reviews*, 14(0):127–139, 1992.
- [18] J. Aboudi, M.-J. Pindera, and Arnold S. M. Linear Thermoelastic Higher-Order Theory for Periodic Multiphase Materials. *Journal of Applied Mechanics*, 68:697–707, 2001.
- [19] E. J. Pineda, B. A. Bednarczyk, A. M. Waas, and S. M. Arnold. Progressive failure of a unidirectional fiber-reinforced composite using the method of cells: Discretization objective computational results. *International Journal of Solids and Structures*, 50(9):1203–1216, 2013.
- [20] C. T. Sun and R. S. Vaidya. Prediction of composite properties from a representative volume element. *Composites Science and Technology*, 56(2):171–179, 1996.

- [21] C. Heinrich, M. Aldridge, A. S. Wineman, J. Kieffer, A. M. Waas, and K. Shahwan. The influence of the representative volume element (RVE) size on the homogenized response of cured fiber composites. *Modelling and Simulation in Materials Science and Engineering*, 20(7):075007, 2012.
- [22] W. Yu and T. Tang. Variational asymptotic method for unit cell homogenization. *Solid Mechanics and its Applications*, 168:117–130, 2010.
- [23] T. M. Ricks, T. E. Lacy, E. J. Pineda, B. A. Bednarczyk, and S. M. Arnold. Computationally efficient High-Fidelity Generalized Method of Cells micromechanics via order-reduction techniques. *Composite Structures*, 156:2–9, 2016.
- [24] E. Carrera, M. Cinefra, E. Zappino, and M. Petrolo. *Finite Element Analysis of Structures Through Unified Formulation*. 2014.
- [25] E. Carrera and M. Petrolo. Refined beam elements with only displacement variables and plate/shell capabilities. *Meccanica*, 47(3):537–556, 2012.
- [26] M. Maiarú, M. Petrolo, and E. Carrera. Evaluation of energy and failure parameters in composite structures via a Component-Wise approach. *Composites Part B: Engineering*, 108:53–64, 2017.
- [27] E. Carrera and G. Giunta. Refined Beam Theories Based on a Unified Formulation. *International Journal of Applied Mechanics*, 02(01):117–143, 2010.
- [28] A. Pagani, A.G. de Miguel, M. Petrolo, and E. Carrera. Analysis of laminated beams via Unified Formulation and Legendre polynomial expansions. *Composite Structures*, 156:78 – 92, 2016.
- [29] A. Pagani, M. Petrolo, G. Colonna, and E. Carrera. Dynamic response of aerospace structures by means of refined beam theories. *Aerospace Science and Technology*, 46:360 – 373, 2015.
- [30] E. Carrera and M. Filippi. A refined one-dimensional rotordynamics model with three-dimensional capabilities. *Journal of Sound and Vibration*, 366:343–356, 2016.
- [31] A. Pagani and E. Carrera. Unified formulation of geometrically nonlinear refined beam theories. *Mechanics of Advanced Materials and Structures*, In Press.
- [32] A. Pagani and E. Carrera. Large-deflection and post-buckling analyses of laminated composite beams by Carrera Unified Formulation. *Composite Structures*, 170:40–52, 2017.

- [33] E. Carrera, A. Pagani, M. Petrolo, and E. Zappino. Recent developments on refined theories for beams with applications. *Mechanical Engineering Reviews*, 2(2):1–30, 2015.
- [34] J.N. Reddy. *Mechanics of laminated composite plates and shells. Theory and Analysis*. CRC Press, 2<sup>nd</sup> edition, 2004.
- [35] K. J. Bathe. *Finite Element Procedures*. Prentice Hall, USA, 1996.
- [36] Z. Xia, Y. Zhang, and F. Ellyin. A unified periodical boundary conditions for representative volume elements of composites and applications. *International Journal of Solids and Structures*, 40(8):1907–1921, 2003.
- [37] K. P. Walker, A. D. Freed, and E. H. Jordan. Accuracy of the Generalized Self-Consistent Method in Modelling the Elastic Behaviour of Periodic Composites. *Philosophical Transactions of the Royal Society A: Mathematical, Physical and Engineering Sciences*, 345(1677):545–576, 1993.